metals

MDPI

Article

Reconstruction of Complex Zygomatic Bone Defects Using Mirroring Coupled with EBM Fabrication of Titanium Implant

Khaja Moiduddin [1,*], Syed Hammad Mian [1], Usama Umer [1], Naveed Ahmed [1,2], Hisham Alkhalefah [1] and Wadea Ameen [1]

[1] Advanced Manufacturing Institute, King Saud University, Riyadh 11421, Saudi Arabia; syedhammad68@yahoo.co.in (S.H.M.); uumer@ksu.edu.sa (U.U.); anaveed@ksu.edu.sa (N.A.); halkhalefah@ksu.edu.sa (H.A.); wqaid@ksu.edu.sa (W.A.)

[2] Department of Industrial and Manufacturing Engineering, University of Engineering and Technology, Lahore 54000, Pakistan

* Correspondence: khussain1@ksu.edu.sa; Tel.: +966-11-469-7372

Received: 17 October 2019; Accepted: 18 November 2019; Published: 22 November 2019

Abstract: Reconstruction of zygomatic complex defects is a surgical challenge, owing to the accurate restoration of structural symmetry as well as facial projection. Generally, there are many available techniques for zygomatic reconstruction, but they hardly achieve aesthetic and functional properties. To our knowledge, there is no such study on zygomatic titanium bone reconstruction, which involves the complete steps from patient computed tomography scan to the fabrication of titanium zygomatic implant and evaluation of implant accuracy. The objective of this study is to propose an integrated system methodology for the reconstruction of complex zygomatic bony defects using titanium comprising several steps, right from the patient scan to implant fabrication while maintaining proper aesthetic and facial symmetry. The integrated system methodology involves computer-assisted implant design based on the patient computed tomography data, the implant fitting accuracy using three-dimensional comparison techniques, finite element analysis to investigate the biomechanical behavior under loading conditions, and finally titanium fabrication of the zygomatic implant using state-of-the-art electron beam melting technology. The resulting titanium implant has a superior aesthetic appearance and preferable biocompatibility. The customized mirrored implant accurately fit on the defective area and restored the tumor region with inconsequential inconsistency. Moreover, the outcome from the two-dimensional analysis provided a good accuracy within 2 mm as established through physical prototyping. Thus, the designed implant produced faultless fitting, favorable symmetry, and satisfying aesthetics. The simulation results also demonstrated the load resistant ability of the implant with max stress within 1.76 MPa. Certainly, the mirrored and electron beam melted titanium implant can be considered as the practical alternative for a bone substitute of complex zygomatic reconstruction.

Keywords: zygomatic bone; customized reconstruction; electron beam melting; 3D comparison; titanium alloy; finite element analysis

1. Introduction

Advancements in the field of biomaterials, fabrication techniques, and computer-assisted technologies have been taking place owing to the huge demand for medical implants [1]. Biomaterials are natural or artificial materials that are used to enhance or replace any tissue, organ, or biological structure in order to improve the quality of human life [2]. Titanium and its alloys have a unique

combination of high strength to low weight ratio, low density and better corrosion resistance, are biocompatible, and have non-magnetic properties. They are one of the few biomaterials that naturally match the requirement of bone tissue replacement in the human body. Among them, commercial pure titanium (grade 2), Ti-6Al-4V (grade 5), and Ti-6Al-4V ELI (Extra low interstitial) (grade 23) are widely used biomaterial in medical application [3]. In addition, a significant rise in the fabrication of custom-built titanium implants with better design and biomechanical properties has been realized in clinical applications. The facilitation and application of tailor-made effective implants are crucial to improve the quality of the patient's life. Moreover, it is of utmost importance to study the implant concerning its design, fitting accuracy, biomechanical properties, and fabrication method.

Zygomatic bone reconstruction is indeed a challenging procedure for maxillofacial surgeons due to its unique position which is close to the orbital rim that houses the eyeball [4]. The integrity of the zygomatic reconstruction can be achieved through the maintenance of the person's aesthetic appearance, its functionality, and the prominence of the cheek [5]. The zygomatic bone is highly robust and variable in shape. It is located at the crucial junction between the zygomatic arc, orbital wall, and tooth bearing snout. It consists of multiple bone tissues types, namely the cancellous bone which is surrounded by cortical bone shell. The cortical bone was found to be thickest (5.0 mm) in the upper zygomatic bone and thinnest (1.1 mm) at the anterior of maxillary sinus region [6]. In addition, the cortical bone has greater volume fraction in the zygomatic bone than the cancellous bone [7]. Studies indicate that the young modulus of zygomatic bone is in the range from 10.4 GPa to 19.6 GPa, respectively [8]. Titanium implants are commonly used for zygomatic bony reconstruction because they provide reliable support for the orbital contents [9]. The first zygomatic implant reconstruction was developed by Branemark without grafting procedures for maxillectomized patients [10]. Different surgical approaches and treatments have been employed since then, for successful zygomatic complex reconstruction, including osteotomy, autologous bone graft, and synthetic implants [11]. Among all, the autologous bone graft is considered gold standards; however, limited bone availability, volatile resorption rate, and deformities remain serious challenges. Hence, various alloplastic implants, including polymers [12], silicone [13], metals [14], and hydroxyapatite based products [15] were also used to replace the autologous bone graft.

Long-term success and effectiveness of the implants depend on several factors, including the design, implant material, accuracy, biomechanical study, fabrication process, and, of course, the skills of the surgeon [4]. In all, the mirror reconstruction technique is one of the widely used implant design techniques for medical applications [16,17]. It can replace the defective bony region with a healthy region, thus maintaining the symmetry and ideal anatomical structure [18]. Titanium alloy (Ti-6Al-4V ELI) is one of the most favored biocompatible materials owing to its high strength to weight ratio, excellent corrosion resistance, and mechanical properties [19]. Titanium and its alloys have excellent biocompatibility when compared to other metallic biomaterials such as stainless steel and cobalt chromium alloys. The most widely used titanium alloy (Ti-6Al-4V ELI) used for bone replacement has a modulus of elasticity (110 GPa) almost half that of stainless steel (200 GPa) and Cobalt chromium alloy (210 GPa) [20]. Development of new titanium alloys with shape memory is a growing attraction for biomedical application with superior elasticity and properties closer to that of bone [21]. One of the important properties that differentiate titanium and its alloys from other biomaterials is the natural formation of thin oxide film on its surface which is responsible for good chemical stability and biocompatibility [22]. The biomechanical study involving stress analysis on the implant and its surrounding bone is also critical to study the orthopedic mechanical failure [23]. It helps to evaluate different designs virtually during functional loading, thus reducing material usage, physical prototyping, and testing methods [24]. Implant accuracy evaluation is also a mandatory procedure to analyze its fitting accuracy. The implant–bone interface contact is necessary for immediate restoration as well as to avoid any damage to the vital structures [25].

Fabrication of an implant from the patient computer tomography (CT) scan involves several steps encompassing data collection and processing, design template, virtual simulation, and fabrication

utilizing three-dimensional (3D) printing. 3D printing also known as rapid prototyping and additive manufacturing is a technique of producing physical 3D objects from computer-aided-design (CAD) files in a successive material layering. Electron beam melting (EBM) is one of the widely used metal 3D printing processes with a US Federal Drug Administration (FDA) approval [26]. It has been widely adopted by surgeons at an impressive rate and is used in a large variety of medical applications [27,28]. The 3D printed models can also be used for mock surgeries, pre-operative planning, surgical guides, and educational training purposes [29].

It is indeed very difficult to reconstruct a complex anatomical structure with proper aesthetic and facial symmetry [30]. Any deviation or aberration in structural alignment between the implant and bone contours may most likely lead to functional disturbance and implant failure. In this study, an integrated methodology involving custom design using the mirror reconstruction technique has been proposed. It also consists of biomechanical evaluation for the custom built implant, implant accuracy assessment using 3D comparison technique, and, finally, the three-dimensional (3D) printing of the titanium implant using state-of-the-art EBM technology. Certainly, the objective is to produce a zygomatic titanium implant, which is reliable based on its functionality, appearance, and mechanical strength. The methodology adopted in this work involves multidisciplinary fields including custom-built design, biomechanical analysis, implant accuracy, and titanium-based EBM fabrication. Most often, the clinicians or engineers, owing to the vastness or intricacies of the field, overlook some important step or assessment test. Henceforth, in this work, the different steps that are pertinent in zygomatic rehabilitation as well as implant realization are comprehensively described.

2. Materials and Methods

The methodology as presented in Figure 1 involved the integration of several technologies to realize the customized zygomatic titanium implant. This approach also comprised of the formal meeting and communication between the engineering department and the medical field in each step, to evaluate and verify the design model for the enhanced aesthetic outcome, and to reduce implant revision and failure. Indeed, a multidisciplinary approach involving biomedical engineers, surgeons, and researchers are vital for the successful fabrication and implementation of implants [31]. Studying implant failure would help the clinicians and engineers in understanding the failure factors and to develop better prosthesis. In this study, a zygomatic implant was first produced using conventional techniques as illustrated in Figure 1a. Later, a new computer-aided custom design implant was produced as shown in Figure 1b and compared with the conventionally produced implant. Some of the drawbacks of conventional techniques in implant design are the excessive time consumption, inaccurate fitting of implant, diagnostic limitations, and lack of surgical planning. From the past decade, the development of computer-assisted implant design and surgical planning has become extremely important in orthopedic surgeries.

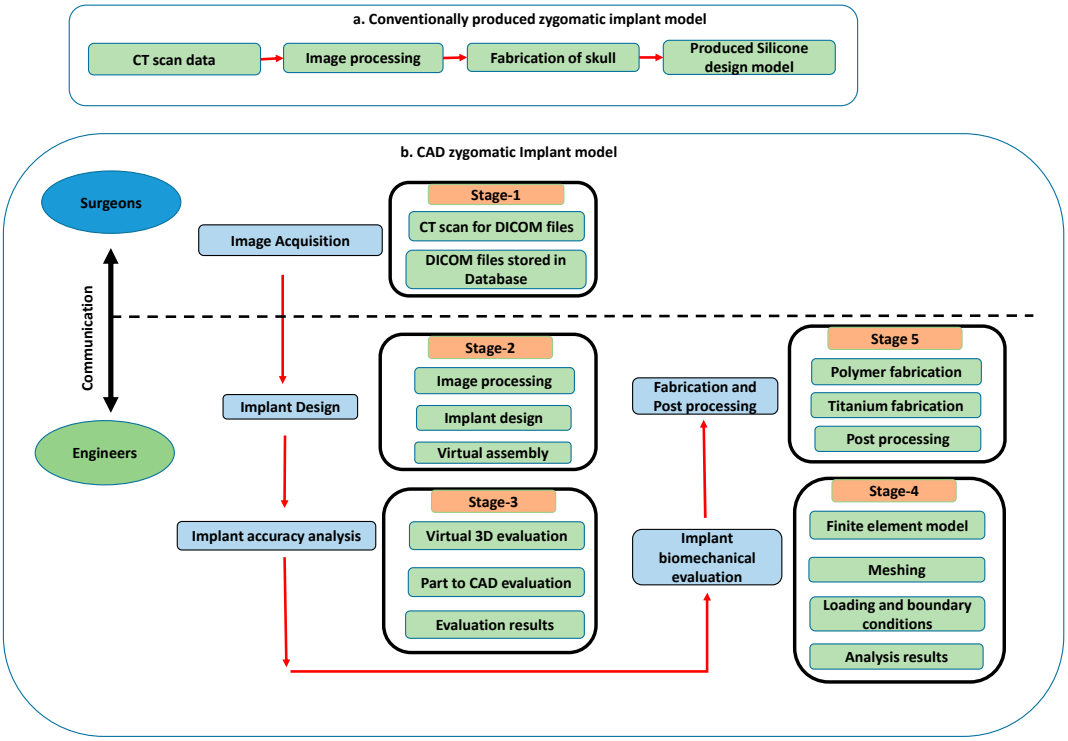

Figure 1. Methodology employed in the fabrication of (**a**) conventionally produced zygomatic implant model and (**b**) computer-aided-design zygomatic implant model.

2.1. Implant Customization and Fabrication

A cone-beam computed tomography (CBCT) scan was performed using Promax 3D (Planmeca, Helsinki, Finland) on a 34-year-old male patient who was suffering from painful cheek swelling. The series of two-dimensional (2D) images obtained from the CT scan were stored as a Digital Imaging and Communications in Medicine (DICOM) file in a database. The DICOM file was then imported into Mimics® (version, Materialise, Leuven, Belgium), a medical modeling software, which distinctly converted the series of 2D images into a 3D model as shown in Figure 2. The thresholding function from Mimics® with a thresholding value of 226 to 3071 Hounsfield Units (HU) was used to segregate the hard and soft tissues. The HU is a universally acceptable dimensionless unit that is used to express CT numbers. The Segmentation and region growing functions using Mimics® were used to divide and subdivide the image into several regions until the region of interest–Skull (green) was obtained. The obtained 3D skull model was then saved as a Standard Translation Language (STL) file and imported into a polymer 3D printer-fused deposition modeling (FDM) for fabrication.

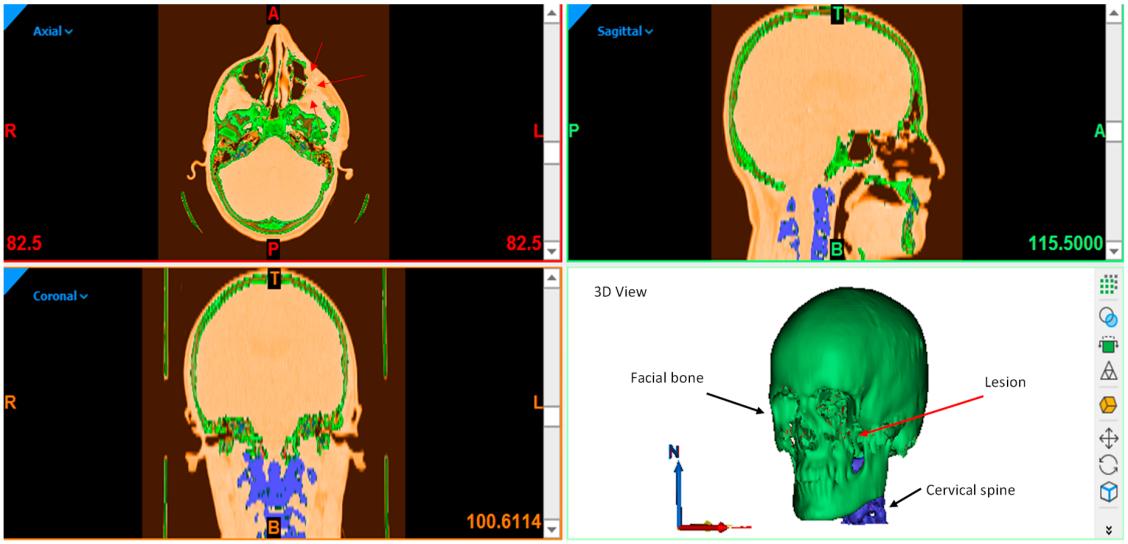

Figure 2. 3D model of the patient skull anatomy revealing the tumor location.

The FDM fabricated skull 3D model was used for designing the zygomatic implant. A silicone impression material was placed over the defective area and gently molded to obtain the shape of the zygomatic bone as shown in Figure 3a. As the process was done manually, a lot of contours and rough surfaces could be observed on the posterior end of the implant (Figure 3c). The conventionally designed implant (Figure 3b) did not adapt to the recipient defect perfectly, and hence it was rejected based on the formal meeting with the medical clinicians. On further discussion with the surgeons, it was decided to have a new CAD implant model using reconstruction techniques.

There are two types of implant reconstruction techniques widely used in custom designs [32]. The first is a mirror reconstruction technique and the other is an anatomical reconstruction design based on a curve based and refinement approach [4]. The mirroring technique provides better facial symmetry and is more accurate for medium and large complex tumors, whereas the anatomical reconstruction technique is a lengthy process, requires lots of human expertise, and provides good results for smaller tumors [33,34]. One of the major differences between these two techniques is that mirroring techniques can be applied only in symmetrical regions, whereas anatomical reconstruction can be applied to both symmetrical and asymmetrical parts.

Figure 3. (**a**) Fused deposition Modeling fabricated skull model with the attached silicone implant; (**b**) silicone implant front view; and (**c**) silicone implant back view.

Based on the inputs from the medical clinicians, an implant mirror reconstruction technique was utilized to replace the defective region with the healthier bony region. The steps involved in the mirroring reconstruction technique are illustrated in Figure 4. Primarily, the STL defective model (Figure 4a) was first resected into two halves (Figure 4b) using Magics® (Materialise, Leuven, Belgium). The defective side was removed (Figure 4c) and replaced by the healthy right side (Figure 4d) using the mirror reconstruction technique. The next step was to join the two error-free sides through merging operation (Figure 4e). Any voids or gaps were removed by wrapping operations (Figure 4f). Boolean subtraction process (Figure 4g) was performed between the error-free model (Figure 4f) and the tumor model (Figure 4a) to obtain the zygomatic implant template (Figure 4h), which was then saved as an STL file for subsequent fabrication.

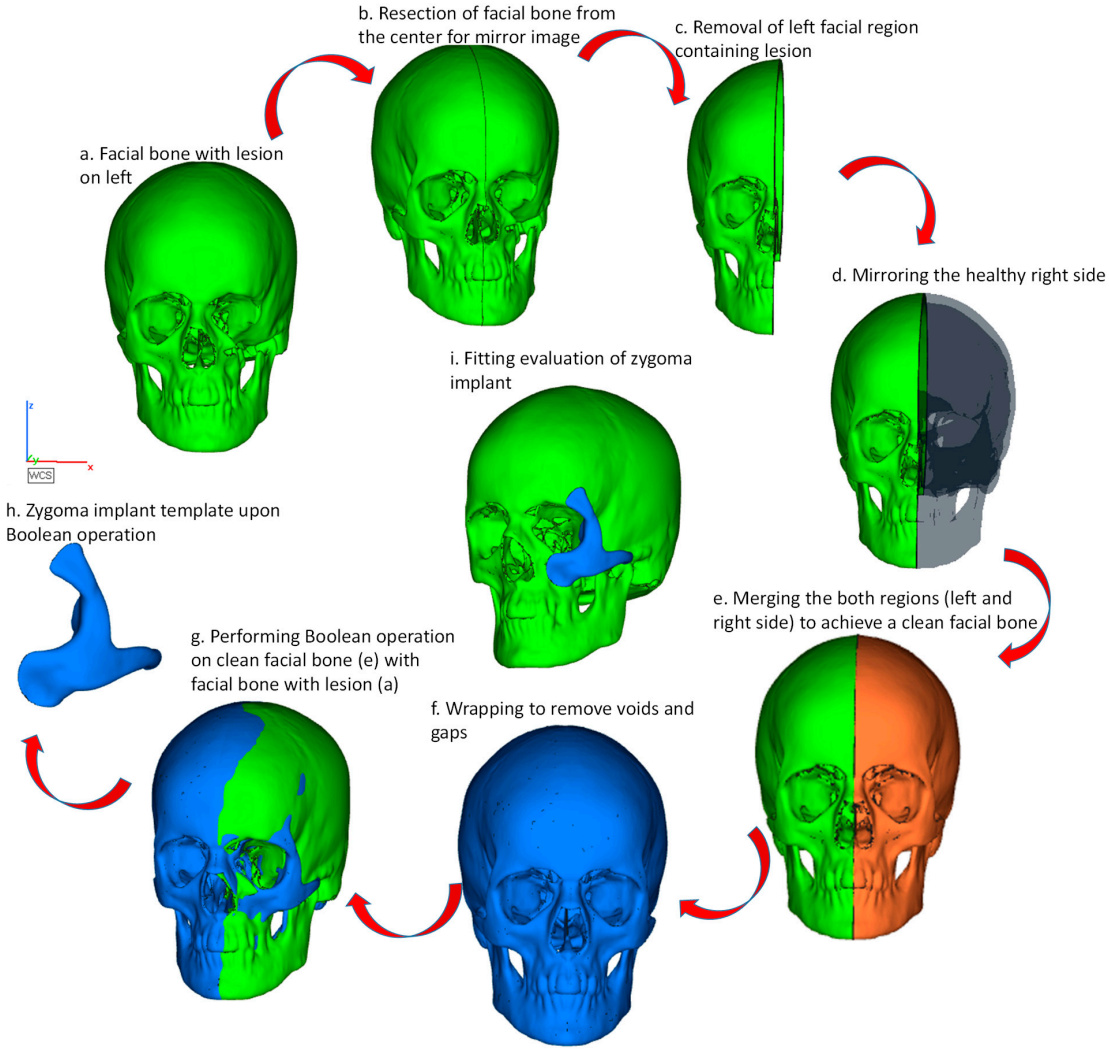

Figure 4. Computer-aided customized zygomatic implant process cycle. (**a**) facial bone with lesion; (**b**) resection of facial bone for mirror image; (**c**) removal of left facial region with lesion; (**d**) mirroring the healthy right side; (**e**) merging both left and right regions to obtain clean facial bone; (**f**) wrapping operation to remove gaps; (**g**) boolean operation between clean facial bone and facial bone with lesion; (**h**) obtained zygomatic bone template upon Boolean operation; (**i**) fitting evaluation of zygoma implant.

Figure 5 illustrates the FDM fabricated zygomatic implant designed using a mirror reconstruction technique as well as its counterpart that is a conventionally produced implant model. On visual observation, it can be clearly seen that the manually produced implant model has lots of curves and rough surfaces when compared to the mirror implant model produced through FDM. Figure 6

demonstrates the precise fitting of the mirror implant model onto the skull model. The polymer produced FDM models also assisted the medical clinicians in comprehensive surgical planning and rehearsal in addition to precise drilling of screw holes.

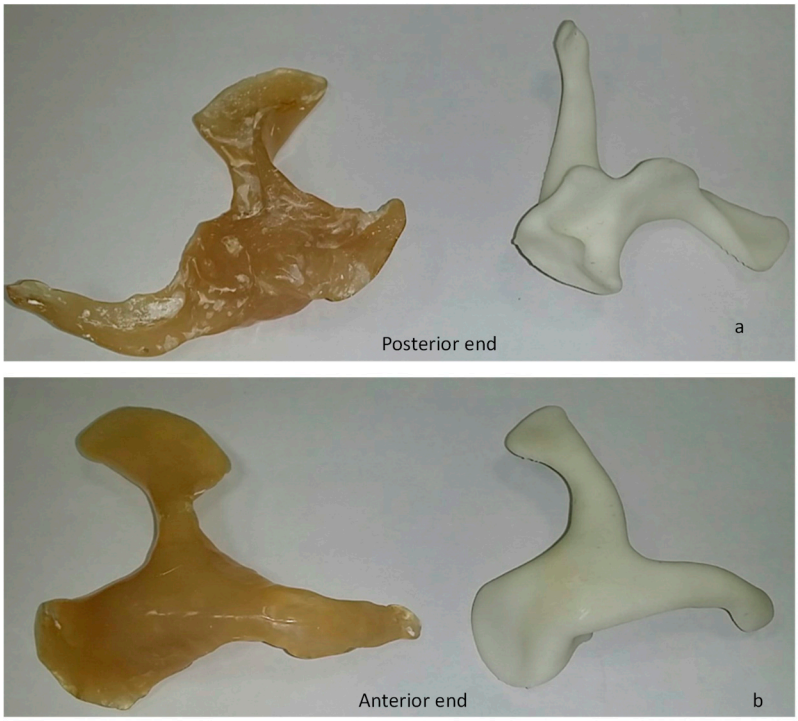

Figure 5. Silicone based zygomatic implant produced manually without CAD technique (**a**) and FDM fabricated zygomatic implant by CAD mirroring technique (**b**).

Figure 6. (**a**) FDM fabricated customized zygomatic implant fitted onto the skull model (front view); (**b**) side view illustration.

After the successful rehearsal and fitting operation of the FDM produced a zygomatic implant onto the skull model and based on the approval from the clinicians, the mirror implant model was fabricated using EBM technology. Arcam's EBM technology offers a new method of rapid manufacturing of near net shaped titanium products, thus eliminating the time, cost and challenges in machining and casting [35]. Arcam EBM A2 machine (Arcam AB, Mölndal, Sweden) as illustrated in Figure 7b was

used for the fabrication of titanium zygomatic implant. The accuracy of the EBM machine is in the range of 0.13 mm to 0.20 mm for shorter to long range build parts and the highest resolution is 50 µm [36,37]. The EBM process cycle is illustrated in Figure 7c where the filament (1), when heated to a temperature of above 2500 °C, accelerates a beam of electron (5) through the series of magnetic lenses including astigmatism lens, focus lens, and deflection lens before hitting the titanium powder (Ti-6Al-4V ELI) (8). The first magnetic lens (2) generates a circular beam of electrons and corrects astigmatism while the second magnetic lens (3) focuses the electron beam to the desired diameter, and the third magnetic lens (4) deflects the focused beam to the desired position. The powder hoppers (6) continuously feed the titanium powder (8) onto the start plate (10) inside the build platform. A mechanical raking blade (7) spreads the titanium powder evenly onto the build platform (9). Initially, a high-speed beam of electrons scans the titanium powder to preheat the powder to a sintered state. After preheating, the melting of powder takes place at slower beam scans. On completion of each melting cycle, the build platform is lowered by one-layer thickness. The entire EBM build process takes place under vacuum and under elevated temperature. This is done to prevent reactions between reactive metals (titanium) with oxygen and to prevent residual stresses [38].

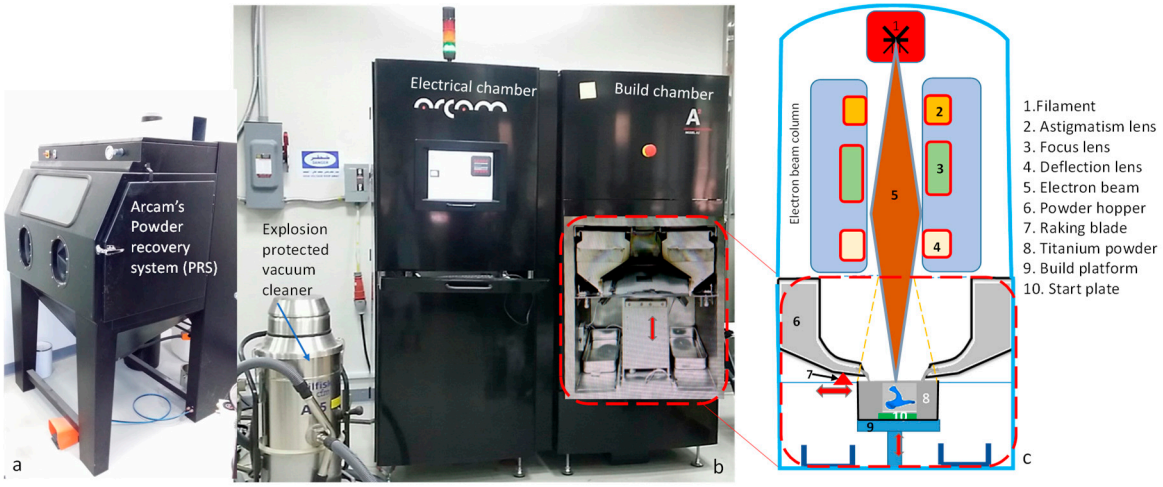

Figure 7. (**a**) ARCAM powder recovery system unit to remove the sintered powder attached to the build part, (**b**) ARCAM A2 electron beam melting machine, and (**c**) the schematic working diagram of electron beam melting machine.

Figure 8a illustrates the fabricated titanium zygomatic implant with support structures. The titanium implant after fabrication was placed inside a powder recovery system (PRS) to remove the semi-sintered powder attached to the implant. The support structures were removed manually using pliers. The titanium zygomatic implant was then fixed onto the polymer skull model for fitting evaluation (Figure 8b).

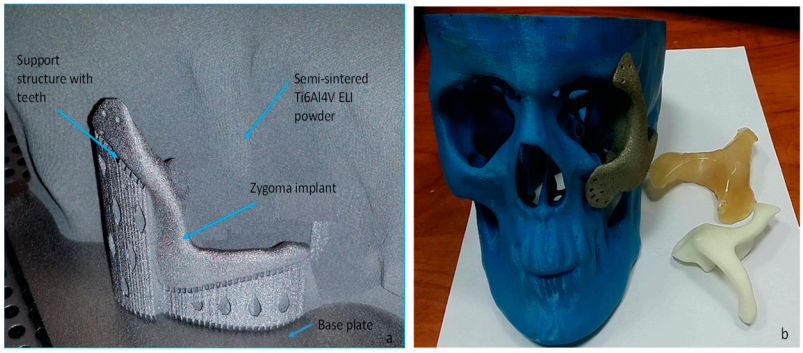

Figure 8. (**a**) EBM fabricated titanium zygomatic implant with support structures inside the powder recovery system and (**b**) titanium zygomatic implant fitted to the skull model after support removal.

2.2. Evaluation

To study the accurate fitting of the implant onto the skull region, an accuracy analysis of the implant was executed in Geomagics Control® (3D systems, Rock Hill, SC, USA). It is one of the most dynamic and comprehensive techniques to estimate the deviation between the test and reference CAD object [39]. It was carried out to quantify the error between the implant and the face model. The implant accuracy analysis was performed in two stages as depicted in Figure 9.

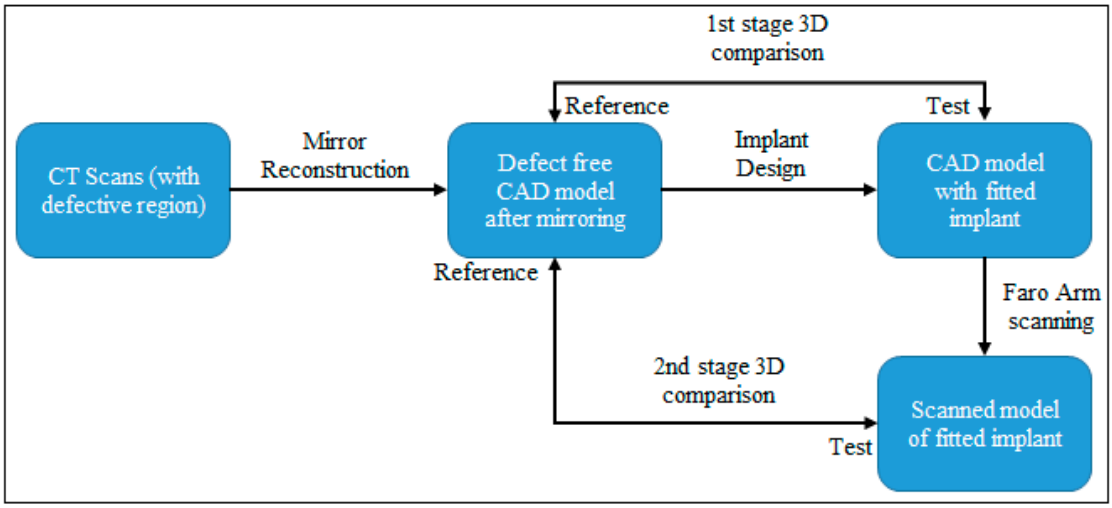

Figure 9. Evaluation of designed implant using comparison approach in Geomagics®.

- First stage comparison before fabrication. In this stage, the tumor-free model after mirroring was taken as a reference and the skull model with the implant was considered as a test file. It was done to quantify the error from the mirroring stage.
- The second stage after fabrication. The 3D model obtained using the Faro platinum arm scanner (FARO, Lake Mary, FL, USA) was used to inspect the implant with the skull model. The 3D model obtained from a Faro arm scanner was considered as a test file and the tumor-free model after mirroring was fixed as the reference file. The test was aligned and superimposed on the error-free mirror model to analyze the deviation error.

The Finite Element Analysis (FEA) was also conducted to investigate the biomechanical behavior of the zygomatic implant and its supporting bone. Typical occlusal loads were applied and stresses on the implants and its surrounding bones were examined. The STL models of Skull and zygomatic implant were first transformed to Solid B-Rep models before analysis. The finite element model (FEM) was developed using ABAQUS/CAE (Version 6.14, Dassault Systemes, Veliez-Villacublai, France).

ABAQUS/CAE is an interactive, graphical environment for Abaqus software. It allows models to be created quickly and easily by producing or importing the geometry of the structure to be analyzed and decomposing the geometry into meshable regions. Once the model is complete, ABAQUS/CAE can submit, monitor, and control the analysis jobs. The Visualization module can then be used to interpret the results. The attributes of cortical bone were assigned to the skull model, and titanium alloy (Ti-6Al-4V ELI) was assigned to the zygomatic implant [40,41]. The material properties designated in the FEA model are presented in Table 1.

Table 1. Material properties utilized in the finite element analysis model [40,41].

Materials	Young's Modulus (GPa)	Poisson's Ratio	Yield Strength (MPa)
Cortical bone	13.7	0.3	122
Zygomatic implant (Ti-6Al-4V ELI)	120	0.3	930

The FEM with load and boundary conditions is shown in Figure 10. The skull was fixed around the neck area and a force of 50 Newton was applied to the zygomatic implant over an area of 500 mm^2. In previous studies, researchers have also applied similar loading conditions of 5.5 kg on zygomatic under the mastication process [42]. The joints between the skull and zygomatic implant were modeled using mesh independent fastener available in ABAQUS/STANDARD. ABAQUS/STANDARD (Version 6.14, Dassault Systemes, Veliez-Villacublai, France) is a general-purpose analysis product that can solve a wide range of linear and nonlinear problems involving the static, dynamic, thermal, electrical, and electromagnetic response of components. Abaqus/Standard solves a system of equations implicitly at each solution increment. Mesh independent fasteners provide a point-based connection between surfaces similar to spot-weld connections. A total of 12 fasteners were utilized across the three joint areas of the zygomatic implant (red-colored) as shown in Figure 10.

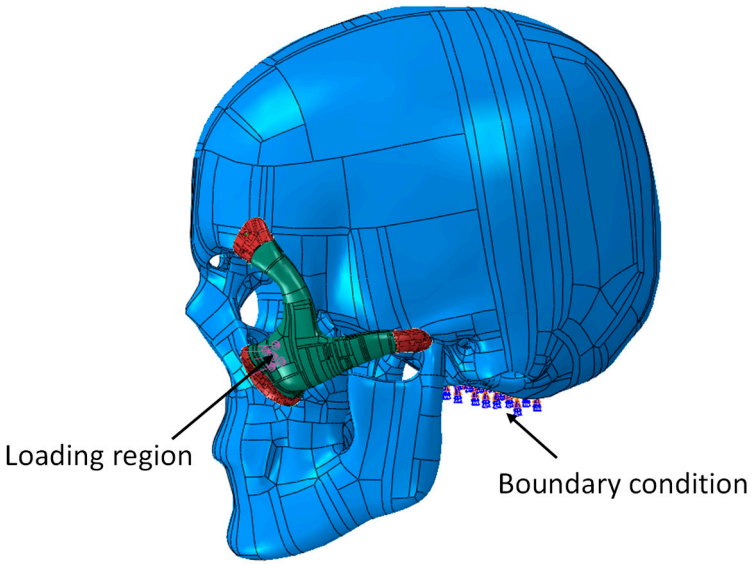

Figure 10. Loading and boundary conditions on the skull and the zygomatic implant.

3D stress quadratic tetrahedron elements (C3D10) with 10 nodes were selected for the FEM as shown in Figure 11. To save computational time, an optimum size mesh is selected that resulted in 149,966 elements in the whole model. To model interaction between implant and skull surfaces, a general contact algorithm has been selected along with frictionless tangential behavior.

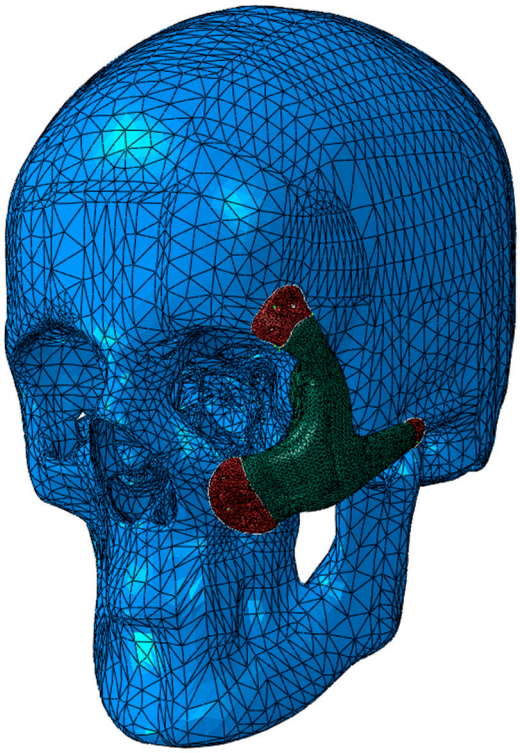

Figure 11. Finite element mesh of the skull and zygomatic implant.

3. Results and Discussion

The tumor-free skull model obtained from the mirror reconstruction technique (Figures 4f and 12b) was used as a reference and the skull model with the attached implant (Figure 12c) was taken as a test file. The test file was aligned and superimposed onto the reference file to obtain the deviation error, which reflected both the mirroring as well as implant shape effect as shown in Figure 12a. In addition to 3D analysis, the 2D comparison was also conducted which quantified the implant shape effect. As it can be observed, there is an inappreciable deviation onto the zygomatic implant region, which states that the obtained zygomatic implant model fitted precisely and replaced the tumor region without much deviation.

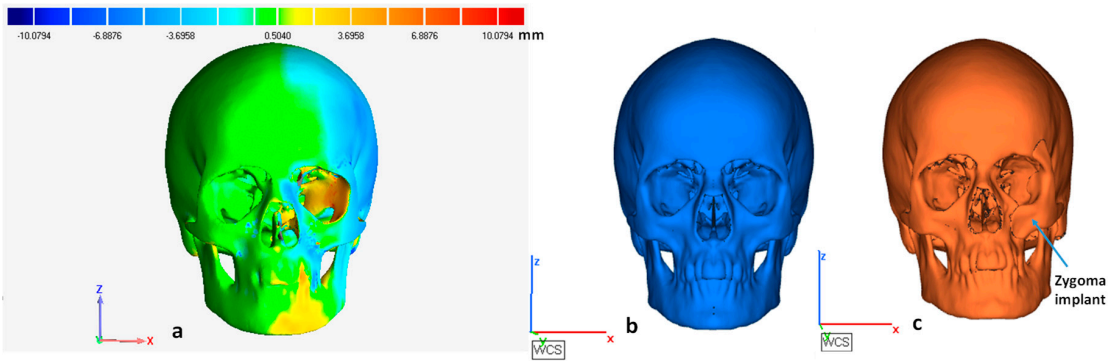

Figure 12. (**a**) 3D inspection results of model deviation between the (**b**) mirror reconstruction model and (**c**) zygomatic implant model.

The 2D comparison results between the reference and the test model are illustrated in Figure 13. In 2D comparison, a cross-sectional plane was created onto the test and reference model in the zygomatic region. Figure 13a–c illustrate the different cross-sectional views of the superimposition of the test file (Figure 13e) onto the reference file (Figure 13d). The color spectrum in the whisker

deviation (Figure 13f) provides the deviation error between them. The 3D and 2D comparison results obtained through virtual model inspection in 1st stage are provided in Table 2.

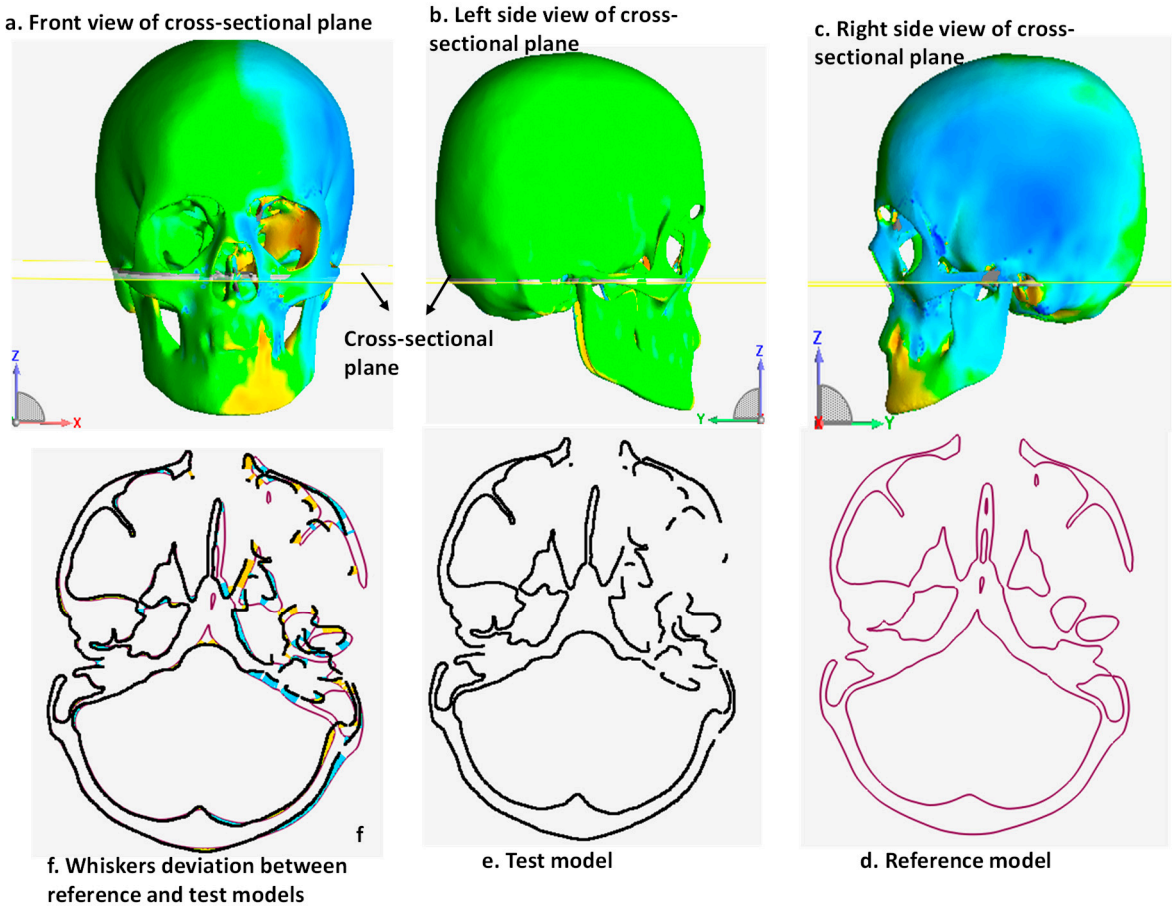

Figure 13. Different views (**a**–**c**) of cross-sectional plane on the implant region. The 2D comparison results (**f**) illustrating the deviation between the (**d**) reference model and the (**e**) test model.

The statistics used to investigate the implant accuracy were the average (AVG) deviation in the positive and negative directions and the root mean square error (RMSE) as illustrated in Equation (1). The average deviation was used as they approximate the differences between the test and reference files in the inward and outward direction. The RMSE represents the average magnitude of the error between two data sets or models. It also quantifies the overall accuracy of the models:

$$\mathrm{RMSE} = \frac{1}{\sqrt{n}} \sqrt{\sum_{i=1}^{n} (X_{1,i} - X_{2,i})^2}, \quad (1)$$

where $X_{1,i}$ is the measurement point of i in the reference data, $X_{2,i}$ is the measurement point of i in the test data, and n is the number of measuring points.

Similarly, the Faro arm scanning and its deviation analysis were carried out on the physical models as shown in Figure 14. The faro arm scanner (Figure 14a) was used to scan the physical facial model attached with an EBM fabricated zygomatic implant. The scanned model was taken as a test file, whereas the mirror reconstruction CAD model was taken as a reference file as illustrated in Figure 14b. The results obtained on the superimposition of test file over a reference file in the 3D comparison technique are shown in Table 2.

Figure 14. 3D measurement (**a**) Faro platinum arm with scanner; (**b**) scanning of the skull model fixed with titanium zygomatic implant.

Table 2. 3D and 2D comparison results for implant accuracy evaluation.

Comparison	Models	AVG Deviation (mm)	Root Mean Square Error (RMSE) (mm)
1st Stage (virtual evaluation using Geomagics®)	Zygomatic mirror and zygomatic with implant (3D comparison)	1.65/–1.55	2.38
	Zygomatic mirror and zygomatic with implant (2D comparison on Implant region)	0.86/–0.97	1.28
2nd Stage (physical model evaluation using Faro arm scanner)	Zygomatic mirror and zygomatic with implant (3D comparison)	1.82/–3.86	4.25
	Zygomatic mirror and zygomatic with implant (2D comparison on Implant region)	1.40/–1.79	1.96

The results from the 1st stage accuracy analysis, where the remodeled or reconstructed face was analyzed with the mirrored face virtually, the average deviation was in the range of 1.65 mm in the outside direction and –1.55 mm in the inward of the face with RMSE as 2.38 mm. In the second stage, when the remodeled physical face model was analyzed with the mirrored face, the average deviation exhibits in the range of 1.82 mm in the outside direction and –3.86 mm in the inward of the face along with RMSE of 4.25 mm. The deviation (or error) was slightly higher in the physical evaluation when compared to virtual evaluation due to the inclusion of several uncertainties from fabrication as well as the scanning procedure performed by the Faro Arm scanner (FARO, Lake Mary, FL, USA). The lesser RSME in 2D comparison of virtual and physical evaluation further validated the implant accuracy for fitting and aesthetic appearance. The 2D comparison was implemented to evaluate the test model at the defect region where the implant was fixed. It did not consider the entire model, but only the region of interest for comparison. Notice that, at this point, it is difficult to establish or compare these results due to the unavailability of similar studies.

This study is the first of its kind where authors have made an effort to quantify the fitting accuracy of the zygomatic implant on the human face. However, the authors along with this analysis also physically anchored the part onto the face to visualize the aesthetics as well as the facial symmetry. The results were satisfactory and acceptable. In addition, the 2D average deviation of physical model with 1.40 mm in the outward direction and −1.79 mm in the inward direction also justify the results—that there is not much deviation at the zygomatic implant. In addition, the authors will carry out similar studies in the future with zygomatic defects to prepare the data for fitting accuracy and determine their acceptable values. As part of the future studies, an in vivo study will also be performed with the zygomatic implant to confirm its fitting performance.

The FEA outcomes can be realized in Figure 15. The Von Mises stress distribution in the model is shown in Figure 15a. Highly stressed regions can be visualized around the joint and contact areas between the skull and the implant. An inverted image of the zygomatic implant is shown in Figure 15b, which identifies different stress regions. Maximum von Mises stress is found to be 1.76 MPa at one of the fastener positions that is well below the yield strength of implant material—thus ensuring the absence of any plastic deformation. Figure 15c shows the maximum principal strain contours for the zygomatic implant. It is clear that high strained regions comprise interaction and fasteners' areas. Nonetheless, these strains are very low and the maximum value approaches 1.34×10^{-5}. The total displacement pattern on the zygomatic implant due to the applied load is shown in Figure 15d. As depicted, maximum displacement occurs at the load-bearing area. However, maximum deformation has been around 2 microns, which again confirms high stiffness of the implant design.

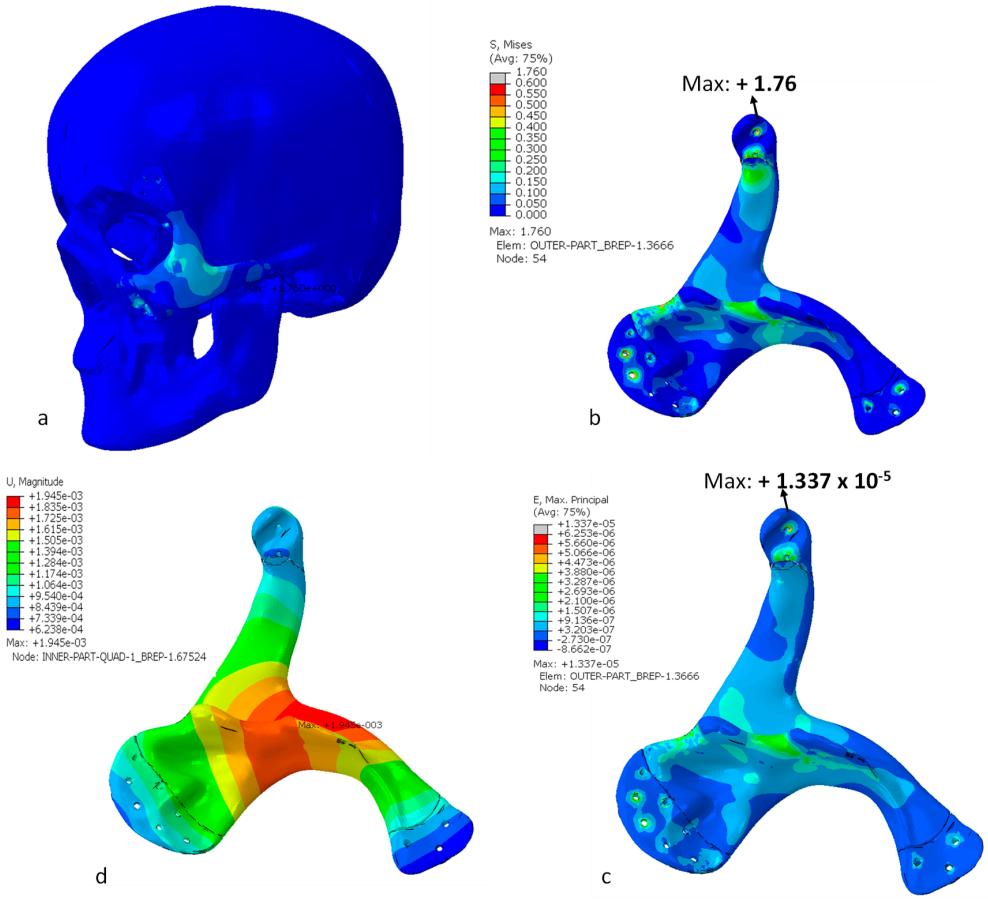

Figure 15. (**a**) Mises stress distributions for the zygomatic implant (MPa), (**b**) Mises stress distributions for the zygomatic implant (MPa), (**c**) maximum principal strain for the zygomatic implant and (**d**) total displacement contour for the zygomatic implant (mm).

4. Conclusions

In this study, a customized zygomatic titanium implant reconstructed using the mirror reconstruction technique was investigated based on the design, biomechanical study, and implant fitting accuracy. The work is particularly important from earlier studies as the authors have identified a technique (2D and 3D comparison) to quantify the implant fitting accuracy or fitting error. Initially, the zygomatic implant was designed manually using silicone, which could not adapt to the bone contours perfectly. Later, a computer-aided custom design implant was constructed using a computer-aided mirroring technique and fabricated using titanium based on state-of-the-art electron beam melting technology. The custom design mirror reconstruction implant precisely fits on the facial region with a maximum deviation error (RMSE) of 2.38 mm in the virtual assembly and 4.25 mm in the physical assembly. Furthermore, the outcomes from the 2D analysis revealed average deviations within 2 mm at the implant region. The implant when practiced on a physical prototype provided a flawless fitting, good symmetry, and pleasant aesthetics. This fitting evaluation study provides crucial information about the implant actualization on the patient's face. This outcome also provides indispensable knowledge for future in vivo or cadaveric implantation studies to further establish the implant's superior performance. The designed implant also successfully withstands the load, with max stress found to be of 1.76 MPa, which is well below the yield strength of implant material (titanium). This proves that the fabricated titanium zygomatic implant possesses the required mechanical strength. Finally, the authors conclude that the EBM fabricated mirror designed titanium implant satisfies the aesthetic, functional, and mechanical properties for efficient zygomatic bone reconstruction. The proposed design methodology can also be applied for other bone reconstruction surgeries. An in vivo or cadaveric based study of the zygomatic titanium implant will be performed as part of future investigation to confirm its fitting performance.

Author Contributions: K.M.: Conceptualization and experiments; K.M. and S.H.M.: Methodology and draft preparation; U.U.: Analysis and Investigation; N.A.: Data curation, resources, and investigation; H.A.: Project administration, revision and funding acquisition, W.A.: Revision and validation.

Funding: This research was financially supported by the Deanship of Scientific Research, King Saud University: Research group No: RG-1440-034.

Acknowledgments: The authors extend their appreciation to the Deanship of Scientific Research at King Saud University for funding this work through Research Group no. RG-1440-034.

Conflicts of Interest: The authors have no conflict of interest to declare.

References

1. Di, M.P.; Coburn, J.; Hwang, D.; Kelly, J.; Khairuzzaman, A.; Ricles, L. Additively manufactured medical products-the FDA perspective. *3D Print Med.* **2016**, *2*, 1–6.
2. de Viteri, V.S.; Fuentes, E. Titanium and Titanium Alloys as Biomaterials. *Tribol. Fundam. Adv. InTech.* **2013**, 155–181.
3. Balazic, M.; Kopac, J.; Jackson, M.J.; Ahmed, W. Review: Titanium and titanium alloy applications in medicine. *IJNBM* **2007**, *1*, 3. [CrossRef]
4. Parthasarathy, J. 3D modeling, custom implants and its future perspectives in craniofacial surgery. *Ann. Maxillofac. Surg.* **2013**, *4*, 9. [CrossRef]
5. Starch-Jensen, T.; Linnebjerg, L.B.; Jensen, J.D. Treatment of Zygomatic Complex Fractures with Surgical or Nonsurgical Intervention: A Retrospective Study. *Int. J. Oral Maxillofac. Surg.* **2018**, *12*, 377–387. [CrossRef]
6. Lee, H.-S.; Choi, H.-M.; Choi, D.-S.; Jang, I.; Cha, B.-K. Bone thickness of the infrazygomatic crest area in skeletal Class III growing patients: A computed tomographic study. *Imaging Sci. Dent.* **2013**, *43*, 261–266. [CrossRef]
7. Pryor McIntosh, L.; Strait, D.S.; Ledogar, J.A.; Smith, A.L.; Ross, C.F.; Wang, Q.; Opperman, L.A.; Dechow, P.C. Internal Bone Architecture in the Zygoma of Human and Pan. *Anat. Rec.* **2016**, *299*, 1704–1717. [CrossRef]

8. Milne, N.; Fitton, L.C.; Kupczik KFagan, M.J.; O'Higgins, P. The role of the zygomaticomaxillary suture in modulating strain distribution within the skull of Macaca fascicularis. *Homo J. Comp. Hum. Biol.* **2009**, *60*, 281.
9. Foletti, J.M.; Martinez, V.; Haen, P.; Godio-Raboutet, Y.; Guyot LThollon, L. Finite element analysis of the human orbit. Behavior of titanium mesh for orbital floor reconstruction in case of trauma recurrence. *J. Stomatol. Oral Maxillofac. Surg.* **2019**, *120*, 91–94. [CrossRef]
10. Parel, S.M.; Brånemark, P.I.; Ohrnell, L.O.; Svensson, B. Remote implant anchorage for the rehabilitation of maxillary defects. *J. Prosthet. Dent.* **2001**, *86*, 377–381. [CrossRef]
11. Quatela, V.C.; Chow, J. Synthetic facial implants. *Facial Plast. Surg. Clin. N. Am.* **2008**, *16*, 1–10. [CrossRef] [PubMed]
12. Scolozzi, P. Maxillofacial reconstruction using polyetheretherketone patient-specific implants by 'mirroring' computational planning. *Aesthetic Plast. Surg.* **2012**, *36*, 660–665. [CrossRef] [PubMed]
13. Ivy, E.J.; Lorenc, Z.P.; Aston, S.J. Malar augmentation with silicone implants. *Plast. Reconstr. Surg.* **1995**, *96*, 63–68. [CrossRef] [PubMed]
14. El-Khayat, B.; Eley, K.A.; Shah, K.A.; Watt-Smith, S.R. Ewings sarcoma of the zygoma reconstructed with a gold prosthesis: A rare tumor and unique reconstruction. *Oral Surg. Oral Med. Oral Pathol. Oral Radiol. Endod.* **2010**, *109*, e5–e10. [CrossRef] [PubMed]
15. Hoffmann, J.; Cornelius, C.P.; Groten, M.; Pröbster, L.; Pfannenberg, C.; Schwenzer, N. Orbital reconstruction with individually copy-milled ceramic implants. *Plast. Reconstr. Surg.* **1998**, *101*, 604–612. [CrossRef] [PubMed]
16. Zhang, Y. Orbital Defect Repair and Secondary Reconstruction of Enophthalmos with Mirror-Technique Fabricated Titanium Mesh. *J. Oral Maxillofac. Surg.* **2008**, *66*, 19–20. [CrossRef]
17. Moiduddin, K.; Mian, S.H.; Umer, U.; Alkhalefah, H. Fabrication and Analysis of a Ti6Al4V Implant for Cranial Restoration. *Appl. Sci.* **2019**, *9*, 2513. [CrossRef]
18. Liu, Y.; Xu, L.; Zhu, H.; Liu, S.S.-Y. Technical procedures for template-guided surgery for mandibular reconstruction based on digital design and manufacturing. *Biomed Eng. Online* **2014**, *13*, 63. [CrossRef]
19. Christensen, A.; Kircher, R.; Lippincott, A. Qualification of electron beam melted (EBM) Ti6Al4V-ELI for orthopaedic implant applications. In *Medical Device Materials IV: Proceedings of the Materials and Processes for Medical Devices Conference*; Jeremy, G., Ed.; ASM International: Cleveland, OH, USA, 2007; Volume 6, pp. 48–53.
20. Niinomi, M. Recent research and development in titanium alloys for biomedical applications and healthcare goods. *Sci. Technol. Adv. Mater.* **2003**, *4*, 445. [CrossRef]
21. Ehtemam-Haghighi, S.; Prashanth, K.G.; Attar, H.; Chaubey, A.K.; Cao, G.H.; Zhang, L.C. Evaluation of mechanical and wear properties of Ti xNb 7Fe alloys designed for biomedical applications. *Mater. Des.* **2016**, *111*, 592–599. [CrossRef]
22. Huynh, V.; Ngo, N.K.; Golden, T.D. Surface Activation and Pretreatments for Biocompatible Metals and Alloys Used in Biomedical Applications. *Int. J. Biomater.* **2019**, *2019*, 21. [CrossRef] [PubMed]
23. Coquim, J.; Clemenzi, J.; Salahi, M.; Sherif, A.; Tavakkoli Avval, P.; Shah, S.; Schemitsch, E.H.; Shaghayegh Bagheri, Z.; Bougherara, H.; Zdero, R. Biomechanical Analysis Using FEA and Experiments of Metal Plate and Bone Strut Repair of a Femur Midshaft Segmental Defect. *Biomed. Res. Int.* **2018**, *2018*, 11. [CrossRef] [PubMed]
24. Lemu, H.G. Virtual engineering in design and manufacturing. *Adv. Manuf.* **2014**, *2*, 289–294. [CrossRef]
25. Shah, F.A.; Thomsen, P.; Palmquist, A. Osseointegration and current interpretations of the bone-implant interface. *Acta Biomater.* **2019**, *84*, 1–15. [CrossRef] [PubMed]
26. Wysocki, B.; Maj, P.; Sitek, R.; Buhagiar, J.; Kurzydłowski, K.; Święszkowski, W. Laser and Electron Beam Additive Manufacturing Methods of Fabricating Titanium Bone Implants. *Appl. Sci.* **2017**, *7*, 657. [CrossRef]
27. Li, X.; Wang, C.; Zhang, W.; Li, Y. Fabrication and characterization of porous Ti6Al4V parts for biomedical applications using electron beam melting process. *Mater. Lett.* **2009**, *63*, 403–405. [CrossRef]
28. Moiduddin, K.; Hammad Mian, S.; Alkindi, M.; Ramalingam, S.; Alkhalefah, H.; Alghamdi, O. An in vivo Evaluation of Biocompatibility and Implant Accuracy of the Electron Beam Melting and Commercial Reconstruction Plates. *Metals* **2019**, *9*, 1065. [CrossRef]
29. Hoang, D.; Perrault, D.; Stevanovic, M.; Ghiassi, A. Surgical applications of three-dimensional printing: A review of the current literature & how to get started. *Ann. Transl. Med.* **2016**, *4*, 456.

30. Lee, J.-W.; Fang, J.-J.; Chang, L.-R.; Yu, C.-K. Mandibular Defect Reconstruction with the Help of Mirror Imaging Coupled with Laser Stereolithographic Modeling Technique. *J. Formos. Med. Assoc.* **2007**, *106*, 244–250. [CrossRef]
31. Kashi, A.; Saha, S. Mechanisms of failure of medical implants during long-term use. In *Biointegration of Medical Implant Materials*; Sharma, C.P., Ed.; Woodhead Publishing: Cambridge, UK, 2010; pp. 326–348.
32. Singare, S.; Shenggui, C.; Sheng, L. The use of 3D printing technology in human defect reconstruction-a review of cases study. *Med. Res. Innov.* **2017**, *1*, 1–4. [CrossRef]
33. Moiduddin, K.; Al-Ahmari, A.; Nasr, E.S.A.; Mian, S.H.; Al Kindi, M. A comparison study on the design of mirror and anatomy reconstruction technique in maxillofacial region. *Technol. Health Care* **2016**, *24*, 377–389. [CrossRef] [PubMed]
34. Jardini, A.L.; Larosa, M.A.; Maciel Filho, R.; de Carvalho Zavaglia, C.A.; Bernardes, L.F.; Lambert, C.S.; Calderoni, D.R.; Kharmandayan, P. Cranial reconstruction: 3D biomodel and custom-built implant created using additive manufacturing. *J. Cranio-Maxillofac. Surg.* **2014**, *42*, 1877–1884. [CrossRef] [PubMed]
35. Lütjering, G.; Williams, J.C. *Titanium*; Springer Science & Business Media: Berlin, Germany, 2007.
36. Arcam, A. Arcam A2 Technical Specification. ARCAM A2 TECHNICAL DATA. 2019. Available online: http://www.arcam.com/wp-content/uploads/Arcam-A2.pdf (accessed on 23 May 2019).
37. New! 50 µm Process for High Resolution and Surface Finish. 21 May 2012. Available online: http://www.arcam.com/new-50-um-process-for-high-resolution-and-surface-finish (accessed on 14 September 2019).
38. Umer, U.; Ameen, W.; Abidi, M.H.; Moiduddin, K.; Alkhalefah, H.; Alkahtani, M.; Al-Ahmari, A. Modeling the Effect of Different Support Structures in Electron Beam Melting of Titanium Alloy Using Finite Element Models. *Metals* **2019**, *9*, 806. [CrossRef]
39. Mian, S.H.; Mannan, M.A.; Al-Ahmari, A.M. The influence of surface topology on the quality of the point cloud data acquired with laser line scanning probe. *Sens. Rev.* **2014**, *34*, 255–265. [CrossRef]
40. El-Anwar, M.I.; Mohammed, M.S. Comparison between two low profile attachments for implant mandibular overdentures. *J. Genet. Eng. Biotechnol.* **2014**, *12*, 45–53. [CrossRef]
41. Arcam, Ti6Al4V ELI Titanium Alloy, Ti6Al4V ELI Titanium Alloy. Available online: http://www.arcam.com/wp-content/uploads/Arcam-Ti6Al4V-ELI-Titanium-Alloy.pdf (accessed on 23 September 2019).
42. Nagasao, M.; Nagasao, T.; Imanishi, Y.; Tomita, T.; Tamaki, T.; Ogawa, K. Experimental evaluation of relapse-risks in operated zygoma fractures. *Auris. Nasus. Larynx.* **2009**, *36*, 168–175. [CrossRef]